Nanoparticle-Based Targeting and Detection of Microcavities

*Nathan A. Jones, Sywe-Ren Chang, William J. Troske, Brian H. Clarkson, and Joerg Lahann**

Although dental caries is the most prevalent oral disease worldwide, currently, many dentists continue to use the traditional mirror and probe (dental explorer) method of caries diagnosis. This method of caries detection has the drawback that it is often difficult to distinguish between active and inactive carious lesions. In this work, novel bio-based nanoparticles are developed to specifically detect active caries in vitro. The nanoparticles are made from a cationic fluorescein-labeled food-grade starch in order to fluoresce when illuminated by a standard dental curing light, and to degrade in the oral cavity into nontoxic compounds after detecting the active carious lesion. When exposed to extracted human teeth, cationic fluorescent (+5.8 ± 1.2 mV) nanoparticles (size 101 ± 56 nm) selectively illuminate active caries, but not the healthy tooth surface. Two-photon microscopy confirms the selective binding and accumulation of cationic fluorescent nanoparticles into microscopic carious pores in enamel. These novel nanoparticles provide a unique method to assist in the early diagnosis of active carious lesions with the potential to directly impact dental treatment.

1. Introduction

The use of nanoparticles for medical applications has garnered considerable interest, particularly for drug delivery, diagnostics, and imaging.[1–3] Oral health applications of nanoparticles have not yet received as much attention, but offer potential for technological advances that can immediately impact patient treatment and outcomes.

N. A. Jones, Prof. J. Lahann
Macromolecular Science and Engineering
University of Michigan
Ann Arbor, MI 48109, USA
E-mail: lahann@umich.edu
N. A. Jones, W. J. Troske, Prof. J. Lahann
Biointerfaces Institute
University of Michigan
Ann Arbor, MI 48109, USA
S.-R. Chang, Prof. B. H. Clarkson
Cariology, Restorative Sciences, and Endodontics, Dental School
University of Michigan
Ann Arbor, MI 48109, USA
W. J. Troske, Prof. J. Lahann
Chemical Engineering
University of Michigan
Ann Arbor, MI 48109, USA

DOI: 10.1002/adhm.201600883

Nearly everyone will develop caries at some point in their life.[4] Worldwide, dental caries is the most prevalent disease with ≈36% of the world's population presenting with active caries. In the US, dental caries is the most common chronic disease and more than 90% of adults will have experienced dental caries in their permanent teeth.[5] The average American adult has 3.3 decayed or missing teeth, and 25.5% of adults have untreated dental caries. Adults and children of lower socioeconomic class have more untreated dental caries, because of lack of access to affordable treatment.[5]

Dental cavities form when bacteria in the dental biofilm on the surface of teeth ferment sugars and produce acids, which demineralize enamel and/or dentin. Generally inactive lesions require no treatment while active lesions do. Early active lesions permit conservative remineralization treatment, while cavitated lesions require dental restoration. An active lesion is one that is progressing and has a slightly decalcified (≈5% compared to normal enamel) microporous surface, overlying a subsurface lesion that may have a porosity as high as 30%–40%.[6,7] In contrast, an inactive lesion is not progressing, because the porosity, particularly on the surface, has been reduced by mineral and/or protein deposition, thus facilitating conservative management. Smaller, early stage active carious lesions, also called "microcavities", incipient carious lesions, or white spot lesions, can be reversed by a process called remineralization, which uses the calcium and phosphorous in the saliva and is aided by the presence of fluoride in drinking water or toothpaste.[7] However, if decalcification continues, irreversible cavitation will occur, requiring a dental procedure to avoid further progression of the carious lesion. If left untreated, caries progression can lead to pain, tooth loss, alveolar bone resorption, and in rare cases, death.

The diagnosis of active dental caries is challenging, as presentation is highly variable.[8–10] Typically, diagnosis of caries is carried out optically and tactically with a dental mirror and explorer using techniques which have not changed in almost a century.[8,9] However, tactile detection of a carious lesion by applying pressure on a dental explorer on a demineralized lesion may lead to cavitation.[9,10] X-ray images of the teeth can be taken to identify cavities, particularly for regions in between teeth (interproximal caries), however, this suffers

from several limitations. X-ray images lack the resolution to identify early forming lesions, which can still be repaired by an improved oral hygiene regimen and a fluoride application.[11] There are several new alternative methods for caries diagnosis that have been developed to address these drawbacks, including fluorescence, optical, radiographic, and electrical conductance methods.[12,13] These methods require additional equipment, show minimal benefit over optical diagnosis, and incur greater cost to dentist and patient.[10,12,13] Most importantly these methods only diagnose a lesion in the enamel surface, but do not distinguish between active and inactive lesions, which is the most critical need in modern cariology.[10]

If active carious lesions can be diagnosed before irreversible cavitation occurs, the patient and dentist can be alerted to improve dental hygiene in specific regions of the mouth. In this study, we have indirectly shown that the carious lesions have a negative surface charge, and therefore cationic nanoparticles may be used for targeting lesions due to electrostatic interactions. To this end, we report a starch-based fluorescently-labeled cationic nanoparticle which selectively adsorbs onto active white spot enamel lesions in vitro. The use of food-grade starch as the base polymer makes the particles nontoxic and biodegradable upon exposure to salivary amylase. Fluorescein was chosen as a fluorophore for its understood safety profile and low toxicity in other diagnostic applications.[14] Using fluorescein, carious lesions can be identified using a standard dental composite curing light, commonly used in dental offices. With further research and following successful clinical studies, these particles could be used by patients as a local application, mouth wash or rinse after cleaning the teeth, and then evaluated by a dentist or dental hygienist with illumination using a standard dental composite curing lamp to identify stained regions as active carious lesions.

In summary, our ultimate goal is to develop a new clinically valid methodology to diagnose early active carious lesions that also enables effective monitoring of conservative treatment. The work reported here establishes the proof-of-principle which demonstrates the potential of this technology. We have developed a nanoparticle technology which specifically targets active carious lesions. The nanoparticles are made from food grade corn starch. We have functionalized them so they specifically target the inside of dental caries. They are tagged with a safe fluorescent dye so the caries will illuminate and be easily seen using a standard dental curing lamp. This would allow dentists to differentiate whether a carious lesion is active or inactive, and could be used to monitor treatment results. The product envisioned is a mouth rinse or local application containing a low concentration of the nanoparticles in water. This would help detect early active carious lesions not visible on the tooth surface, because the extremely small nanoparticles are able to penetrate through surface pores into a very early active lesion. The starch-based nature of these particles allows for rapid degradation by amylase, an enzyme present in human saliva, so teeth will no longer fluoresce upon leaving the dentist's office. With earlier detection of caries and less invasive management, cavitation and expensive treatments will be prevented, resulting in a reduction in dental expenditures by patients, insurance companies, and other payers.

2. Materials

All chemicals were lab grade and purchased from Sigma Aldrich unless otherwise noted. These included tetramethylpiperidinenitroxide (TEMPO), sodium bromide, sodium hypochlorite, isopropyl alcohol, glycidyltrimethylammonium chloride, sodium hydroxide, ethanol, fluoresceinamine isomer 1, 1-ethyl-3-(-3-dimethylaminopropyl) carbodiimide hydrochloride (EDC), *N*-hydroxysuccinimide (NHS), FITC-Dextran (10 K mol. wt.), fluorescein sodium salt, and a Tox8 cell viability assay. Samples of experimental grade starch nanoparticles were provided by EcoSynthetix Inc. (Canada).

3. Results and Discussion

3.1. Chemical Modification and Analysis

The chemical modification of starch nanoparticles followed the approach outlined in **Figure 1**a. The cationic reaction was performed first to effectively modify free hydroxyl groups to make the starch cationic, followed by the TEMPO oxidation of remaining hydroxyl groups. The intention was to create a net positive charge for specific adsorption to carious lesions, while still containing reactive carboxyl groups that allow for subsequent functionalization using EDC/NHS chemistry. Following the steps shown in Figure 1, cationic (StNP-2), anionic (StNP-5), and zwitterionic (StNP-3) particles were prepared. Fourier Transformed Infrared (FTIR) spectra of these particles are shown in Figure 1b. All samples share characteristic bands of the starch backbone, including (C—O) stretching bands at 1154 cm^{-1}, 1121 cm^{-1}, and 1017 cm^{-1}, (CH) stretching bands at 2926 cm^{-1}, and a broad (OH) vibration band centered around 3414 cm^{-1}. There are increased bands at 2932 cm^{-1} (CH alkane), 1450 cm^{-1} (CH alkane), and 1390 cm^{-1} (CH aldehyde) and the appearance of new bands at 2830 cm^{-1} (CH aldehyde), 1720 cm^{-1} (C=O aldehyde), and 1493 cm^{-1} (C—N). These results are consistent with previously reported data on similar reactions.[15,16] The IR spectrum of anionic StNPs indicates a sharp increase of the bands at 1710 cm^{-1} (C=O carboxyl) and 1422 cm^{-1} (—COOH). The zwitterionic StNPs show evidence of all of these bands, suggesting the presence of both carboxyl and cationic functional groups.

To further confirm the cationization of the starch nanoparticles, X-ray photoelectron spectroscopy (XPS) results are shown in Table S1 in the Supporting Information. Nitrogen is unique to the quaternary amine in the cationic starch, and quantification of the nitrogen content allows for determination of the degree of substitution (DS), which has a maximum value of 3.0 for the fully substituted anhydroglucose unit of starch. In cationic StNPs (StNP-2), nitrogen was present after the reaction at ≈1.5–2 atomic percent, which corresponds to an approximate DS of 0.3. This DS is comparable to similarly studied starch cationization reactions.[17,18] The subsequent oxidation did not alter the degree of cationic substitution.

To characterize the TEMPO oxidation reaction, ^1H NMR analysis was performed (Figure S1, Supporting Information).[16] Based on the chemical shift of the C6 proton from 5.2 to 5.4 ppm, we estimate a maximum DS of ≈0.55. It is

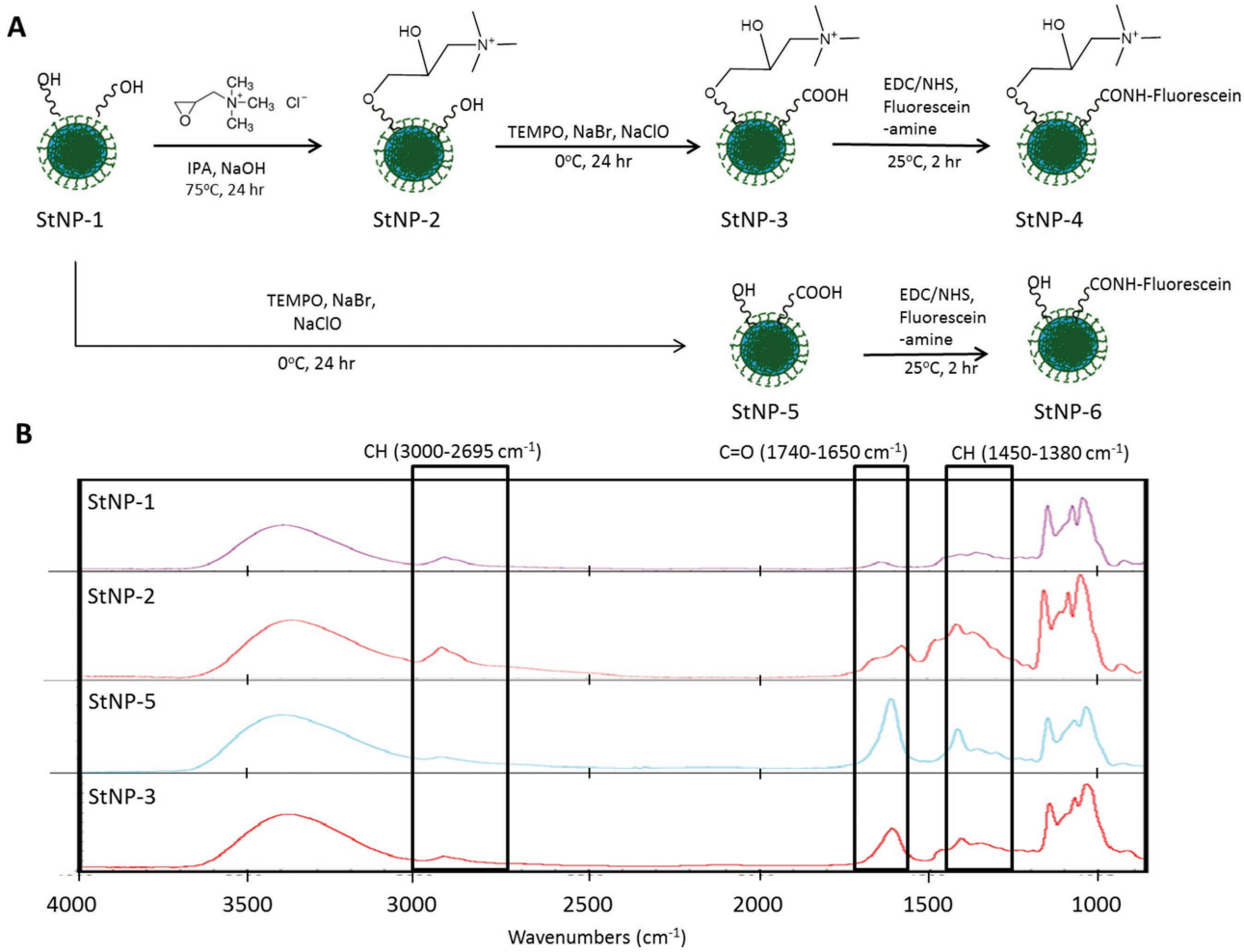

Figure 1. A) Chemical reaction scheme for preparation of starch nanoparticles. Unmodified particles (StNP-1) underwent cationization to prepare cationic particles (StNP-2). TEMPO oxidation on cationic particles (StNP-2) and unmodified particles (StNP-1) yielded zwitterionic particles (StNP-3) and anionic particles (StNP-5), respectively. EDC/NHS chemistry was performed on particles (StNP-3) and (StNP-5) with fluorescein amine to yield cationic fluorescent (StNP-4) and anionic fluorescent (StNP-6) StNP particles, respectively. B) FTIR spectra for unmodified (StNP-1), cationic (StNP-2), anionic (StNP-5), and zwitterionic (StNP-3) starch nanoparticles. Regions of interest for C—H and C=O peaks are highlighted.

hypothesized that the complex gel structure of the starch particles sterically hinders the TEMPO oxidation, and some aldehyde intermediates may be formed.[16]

In addition to the chemical analysis, physical particle analysis was also performed on these samples, including particle size analysis by nanoparticle tracking analysis (NTA) and dynamic light scattering (DLS), as well as zeta potential measurements (**Table 1**). Variation in particle size between NTA and DLS occurs, because NTA provides a number-weighted measurement, while DLS provides an intensity-weighted measurement of particle size. Consequently, DLS measurements of polydisperse or aggregated samples will report larger diameters than the NTA measurements of the same particles.[19] The NTA particle size distributions are shown in Figure S2 in the Supporting Information. Initially, unmodified StNPs (StNP-1) showed a particle size of 41 nm and negligible charge. After TEMPO oxidation (StNP-5), particle charge decreased to –30.5 mV and average particle size decreased to 24 nm. The subsequent reaction with fluorescein via the EDC-NHS reaction reduced the particle charge from –30.5 to –9.3 mV to result in anionic fluorescent StNPs.

In a separate preparation, after cationization (StNP-2), the average particle size decreased to 20 nm and the charge increased to +22.7 mV. For both anionically and cationically modified StNPs, a decrease in particle charge was expected because of the addition of charged modalities on the particle surface, which inhibit aggregation, resulting in an overall decrease in average particle size. When both reactions were combined through TEMPO oxidation of the cationic StNPs, zwitterionic particles were prepared, and the average particle size increased to 101 nm and particles showed a moderate net cationic charge of +8.2 mV. The subsequent reaction with fluorescein via the EDC-NHS reaction reduced the particle charge from +8.2 to +5.8 mV, and appeared to have no significant impact on particle size.

The degradation of starch particles in saliva was demonstrated using iodine and Benedict's reagent tests (**Figure 2**). A colorimetric method of analyzing the iodine solutions was used

Table 1. Particle size and zeta potential results for modified StNPs. Size was measured by intensity-weighted dynamic light scattering and number-weighted nanoparticle tracking analysis.

StNP sample	Zeta potential [mV]	DLS size (Intensity-weighted) [nm]	NTA size (Number-weighted) [nm]
StNP-1 (Unmodified)	–0.6 ± 1.0	53 ± 23	41 ± 28
StNP-5 (Anionic)	–30.5 ± 3.0	90 ± 76	24 ± 17
StNP-6 (Anionic fluorescent)	–9.3 ± 2.3	36 ± 32	45 ± 33
StNP-2 (Cationic)	+22.7 ± 1.3	35 ± 33	20 ± 11
StNP-3 (Zwitterionic)	+8.2 ± 2.0	250 ± 110	101 ± 33
StNP-4 (Cationic fluorescent)	+5.8 ± 1.2	209 ± 110	101 ± 56

instead of direct absorbance measurements to avoid precipitation in the well plates.[20]

UV–vis absorbance measurements were used to quantify the Benedict's test. For unmodified (StNP-1), zwitterionic (StNP-3), and cationic fluorescent (StNP-4) StNPs, the iodine test showed a decrease in starch staining after 30 min of exposure to saliva, while the Benedict's test showed an increase in the presence of reducing sugars. The initial starch–iodine concentration of StNP-1 is higher than the modified nanoparticles (StNP-3 and StNP-4) because the modifications to the starch chemistry inhibit the ability of the iodine to interact with the starch.[21] Similarly, with Benedict's test the modified starches yield fewer reducing sugars, because the starch modification prevents degraded sugars from reducing the Benedict's copper reagent. Nevertheless, these results indicate that starch particles are degraded into reducing sugars after a 30 min exposure to saliva. Based on these data, we concluded that the starch particles can degrade in the patient's mouth within less than an hour after they have been used by the dentist for diagnosis.

The results from the Tox8 cellular toxicity assay are shown in Figure S3 in the Supporting Information. These results indicate that all the particles were nontoxic even at high concentrations of 0.01 g mL^{-1}.

3.2. Dental Activities Testing

Initial testing compared fluorescein sodium salt, fluorescent FITC-dextran, anionic fluorescent StNP, and cationic fluorescent StNP dispersions at selectively targeting carious lesions. A 0.01 g mL^{-1} solution of fluorescein sodium salt nonspecifically (adsorbed to) dyed the tooth (surface); therefore the concentration of fluorescein was reduced to 10^{-5} g mL^{-1}. After rinsing for 20 s, the fluorescein, fluorescent FITC-dextran, and anionic fluorescent StNP control groups displayed no observable levels of fluorescence. In contrast, the cationic fluorescent StNP sample fluorescently illuminated the carious lesions, and rinsing with DI-water for up to 5 min was unable to remove the fluorescence, suggesting specific adsorption of the nanoparticles to the surface of the carious enamel pores. This provided indirect evidence that the active carious lesions have a negative surface charge, and can be specifically targeted with cationic nanoparticles. Similar rinse studies were repeated with saline solutions, and artificial saliva, yielding consistent results.

To validate the efficacy of the cationic fluorescent StNPs, testing was done on the same teeth, using first the controls, rinsing for 30 s, and repeating testing on the same lesion with cationic fluorescent StNPs. Photographs were taken of the teeth, and modified from full-scale lighting to extract the green pixels, as this was found to significantly increase the contrast between lesion and background. The carious lesions are initially slightly darker than the rest of the tooth, and this result is consistent across all controls. The same teeth, treated with the cationic fluorescent StNPs showed fluorescence in the carious lesion region, which was brighter than the background. To quantitatively analyze the images, brightness was measured using ImageJ software. The data are presented with associated pictures in **Figure 3** as an intensity difference comparing the carious lesion to the adjacent region of healthy tooth. Positive values indicate that the carious lesion is brighter than the background tooth, and negative values indicate that the carious lesion is darker than the background tooth. Statistical analysis confirms that untreated teeth are

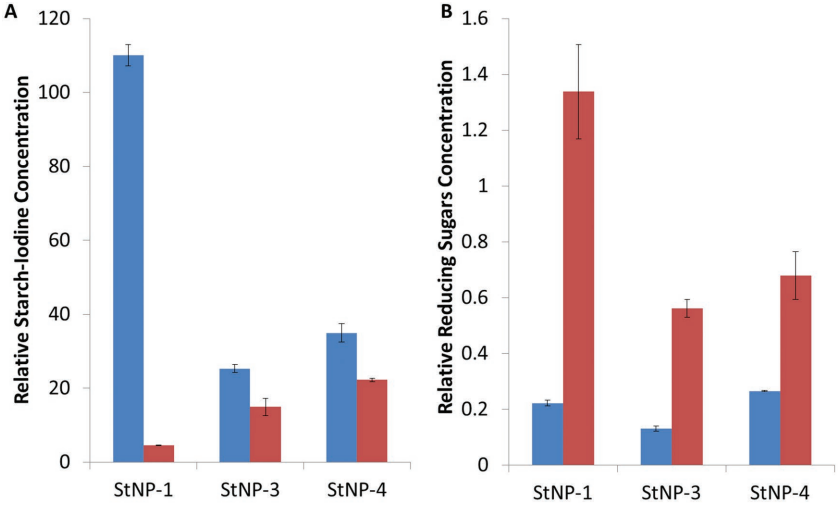

Figure 2. Starch degradation results for StNP-1 (unmodified), StNP-3 (zwitterionic), and StNP-4 (cationic fluorescent) starch nanoparticles, showing levels of starch–iodine complex in (A) and reducing sugars content by Benedict's test in (B). Both graphs show initial levels, in blue, and a final measurement, in red, after 30 min of exposure to salivary amylase in human saliva. A) The iodine concentration is a measure of red intensity, which decreases from initial to final states when exposed to saliva, indicating degradation of starch. The Benedict's reaction was measured by comparing absorption values at 575 nm and shows an increase in absorption after degradation by saliva, indicating the presence of reducing sugars. Results show that in the presence of saliva, starch and modified starch nanoparticles are degraded into simple sugars. ($p < 0.005$ for all initial (blue) vs final (red) comparisons).

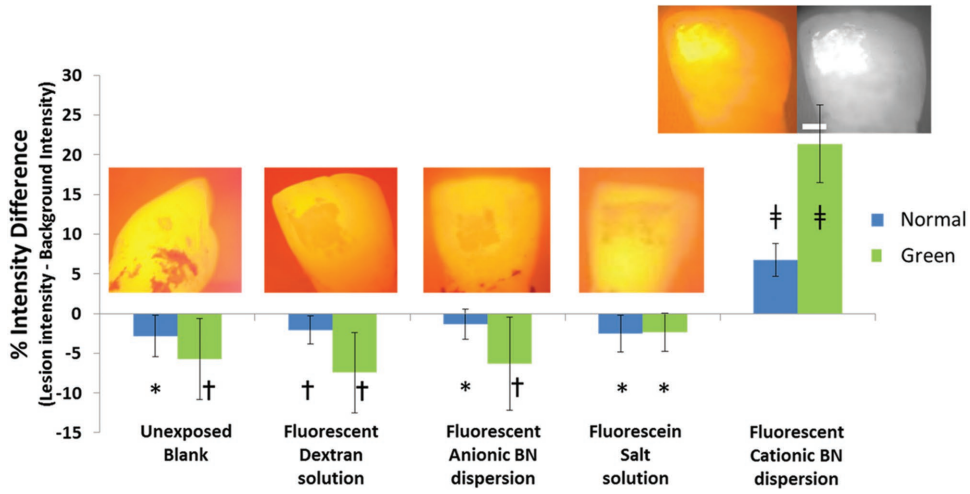

Figure 3. Bar graph showing the contrast of carious lesions for various starches as compared to controls, demonstrating positive contrast for the StNP-4 sample. The teeth were illuminated using a standard dental composite curing lamp. "Normal" stands for the percent intensity difference obtained for unmodified images, and "Green" stands for the extracted green pixel images. Orange inserts show the normal light image, and an example of an extracted green pixel image is shown for the StNP-4 sample. Statistical marks as follows: * Negative contrast ($0.05 < p < 0.20$); †Significant negative contrast ($p < 0.05$); ‡Significant positive contrast ($p < 10^{-5}$).

indistinguishable from fluorescein, fluorescent FITC-dextran, and anionic fluorescent StNP controls, meaning that these controls did not illuminate carious lesions. The analysis further suggests that untreated carious lesions are slightly distinguishable against the background tooth; however, this is not always statistically significant. In stark contrast, the teeth treated with cationic fluorescent StNPs yielded highly significant positive intensity differences ($p < 10^{-5}$), indicating that these particles improved the contrast of carious lesions relative to the background, even to the naked eye. Additionally, analyzing extracted green-pixel images instead of standard RGD images further improved the contrast. It is interesting to note that comparing the nonilluminated images to the illuminated images highlights differences between the delineated shape of the lesion depending on the optical method used (e.g., image of carious lesions treated with anionic fluorescent particles and corresponding image of lesions treated with cationic fluorescent particles). Conceivably, this variation occurs, because the fluorescent particles will only illuminate an active carious lesion with open porosity, while the closed pores of inactive lesions cannot be detected by the starch nanoparticles. In contrast, the nonilluminated lesion images are darker if there is subsurface porosity. This approach thus fails to identify inactive caries due to their closed surface porosity. The ability to distinguish between active and inactive lesions is a significant dental advantage of targeted nanoparticles compared to other diagnostic methods. As a further validation of these results, images of the same teeth were taken using a fluorescent scanner with a green 542 nm bandpass filter and blue light illumination. This method was not chosen as the primary method of analysis, because of its limited translatability, though it significantly increased the contrast compared to the optical method and images obtained by camera using a dental curing light ($p < 10^{-5}$). Nevertheless these results provide further confirmation that the fluorescence seen in the carious lesions is due to the cationic fluorescent starch nanoparticles. Consequently, the prepared cationic fluorescent starch nanoparticles can specifically highlight active caries lesions when illuminated with a standard dental curing lamp in vitro, and offer a simple method to assist dentists in diagnosis of white spot carious lesions.

3.3. Analysis of Nanoparticle Distribution using Two-Photon Microscopy

To dissect the microscopic distribution of nanoparticles in microcavities, two-photon microscopy images of the different conditions were obtained as shown in **Figure 4**. Images show regions of teeth that are 256 × 256 µm across, with depths ranging from 40 to 80 µm gated to capture all detectable fluorescence signals. The various control samples (untreated lesion, or lesion treated with fluorescent FITC-dextran, anionic fluorescent StNPs, or fluorescein sodium salt, or nonlesion treated with cationic fluorescent StNPs) display only low levels of signal due to the autofluorescence of enamel. Darker regions in the control images of carious lesions can be attributed to the porosity of the lesion and may explain their darker macroscopic appearance compared to nonlesion regions of the same tooth. In comparison, the two-photon micrograph of lesions exposed to cationic fluorescent StNPs shows illuminated small pores in the tooth surface of the early carious lesions, resulting in an overall speckled appearance. These results demonstrate, on a microscopic level, the ability of cationic fluorescent starch particles to penetrate and adsorb specifically to the subsurface pores of active carious lesions. An important control is the cationic fluorescent starch nanoparticles on a noncarious surface which showed low brightness typical of enamel autofluorescence similar to the negative controls on caries lesions, validating the selectivity of the cationic starch particles on a microscopic scale. Ring-shaped illumination patterns such as the one shown in

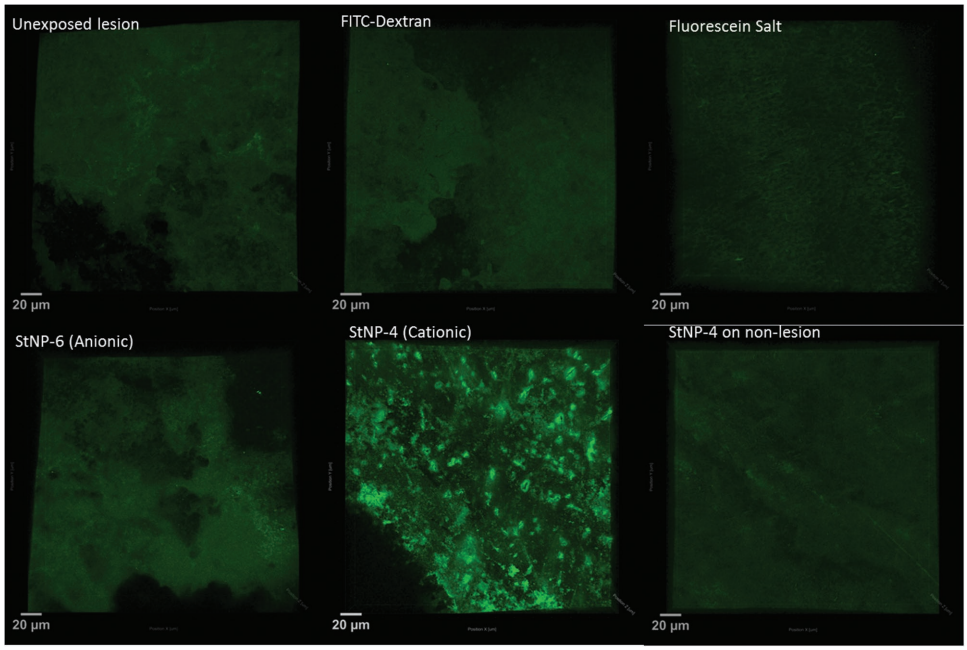

Figure 4. Representative top-view two-photon *z*-stack images of the surface of carious lesions with respective dyes. The lesion unexposed to fluorescent materials has a low fluorescence intensity, similar to the fluorescent FITC-dextran, fluorescein, anionic fluorescent StNP, and cationic nonlesion controls. The sample treated with cationic fluorescent StNPs had a speckled appearance, with bright spots identifying carious lesions on the order of 5–10 µm in diameter and with depths of 5–20 µm.

the inset in **Figure 5** suggest that particles are arranged on the surface of carious pores penetrating into the enamel. Furthermore, the architecture of the pores indicates a larger subsurface porosity covered by a more limited surface porosity, consistent with previously reported studies.[6,7] These results demonstrate that two-photon microscopy can be used to obtain information about the size and shape of illuminated carious lesions, and provide an interesting experimental method in support of carious lesion development and remineralization studies. For example, the carious lesions shown in Figure 5 have an average subsurface diameter of 8.5 ± 6.6 µm, an average depth of 10.3 ± 2.9 µm, and an overall porosity of 14 ± 2%. Monitoring porosity in this manner for different tooth conditions could provide a valuable research tool.

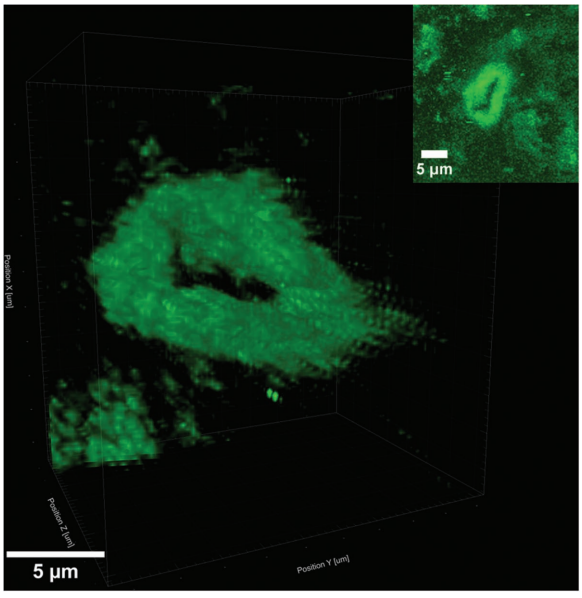

Figure 5. Example of carious lesion pore architecture illuminated by cationic fluorescent StNPs. Particles adsorb to the lumen surface of the pore leaving a central gap. Carious lesion is ≈10 µm wide, by 8 µm deep.

3.4. Nanoparticle Targeting to Remineralized Lesions

Teeth with microcavities were remineralized using a fluoride solution to "heal" the surface porosity of the carious lesions, yielding inactive lesions with subsurface porosity.[22] These lesions were analyzed using the same illumination and image analysis protocols before and after remineralization. The results obtained with a fluorescent scanner are shown in **Figure 6**. By appearance, the remineralized (inactive) lesions were visually indistinguishable from demineralized (active) lesions (inset image in Figure 6). Furthermore, without illumination by cationic fluorescent StNPs, the active and inactive carious lesions are indistinguishable ($p = 0.44$). In contrast, after exposure to cationic fluorescent StNPs, the inactive lesions show only minimal illumination ($p = 0.38$), when compared to active lesions ($p < 10^{-5}$). Though a low level of fluorescence was detected for the remineralized lesions, this is most likely because the teeth were not fully remineralized during the remineralization protocol. However, in all cases, the illumination was lower for the remineralized lesions. Fundamentally, these results validate

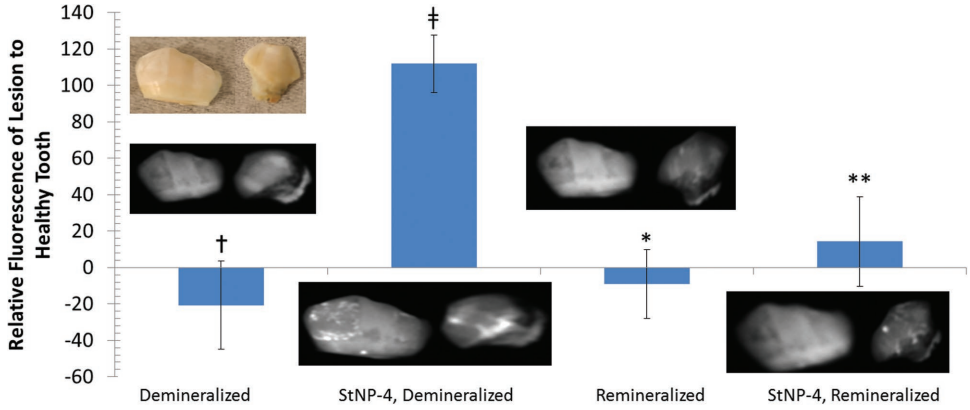

Figure 6. Remineralized (inactive) carious lesions do not illuminate after exposure to cationic fluorescent StNPs, in contrast to demineralized (active) carious lesions. * Negative contrast ($0.05 < p < 0.20$), ** Positive contrast ($0.05 < p < 0.30$), † Significant negative contrast ($p < 0.05$), ‡ Significant positive contrast ($p < 10^{-5}$).

the high degree of specificity of cationic fluorescent StNPs to diagnose and differentiate between active and inactive carious lesions. Use of a specific fluorescent nanoparticle probe can identify caries activity by virtue of surface porosity, which, in active carious lesions allows for diffusion to the subsurface pores, but prevents access to the fluorescent probe in the case of inactive lesions. Clinically, a dentist does not need to treat inactive lesions, and treatments such as fluoride varnishes, gels, washes, or sealants, will have no beneficial effect. In contrast, active lesions are progressing, and appropriate treatment can halt and reverse demineralization. Two-photon micrographs of the remineralized lesions, both before and after exposure to cationic fluorescent StNPs, further support these results (Figure S4, Supporting Information). These images show a smooth surface with no observable fluorescent pores, which most closely resemble a nonlesion surface after exposure to cationic fluorescent StNPs. These results highlight that the remineralized lesion, from a surface perspective, has been healed. Furthermore, dentists and clinical researchers could use the cationic fluorescent StNPs to validate and monitor effective remineralization of carious lesions after treatment, or as a compelling means of quantifying the efficacy of various treatments.

4. Conclusion

We report a novel type of starch-based cationic fluorescent nanoparticles which target and illuminate early forming active carious lesions in vitro. The nanoparticles made from food grade starch, are biodegradable, biocompatible, and are enzymatically degraded in saliva after use. Our ultimate goal is to develop a new clinically valid methodology to diagnose early and active carious lesions that also enables effective monitoring of conservative treatment. With further research and clinical studies, these particles could be used by a dentist or dental hygienist as a local application, mouth wash, or rinse which can then be illuminated using a standard dental curing light used in dental practices, and thus improve the detection of microcavities while they are still reversible by improved dental hygiene and targeted fluoride treatments. Using image analysis, and in particular by analyzing the green colors in images, these particles significantly improve the contrast of carious lesions. Furthermore, two-photon microscopy of teeth treated with these nanoparticles allows for analysis of the microscopic architecture of these lesions. Cationic fluorescent starch nanoparticles have the potential to be used for diagnosis of early caries in dental clinics, for point-of-care use, or to monitor tooth remineralization therapies. These novel nanoparticles provide a unique method to assist in the early diagnosis and treatment of active carious lesions. Similarly designed nanoparticles could be used to deliver fluoride, other remineralization aides, or antibacterial therapeutics to help improve dental health.

5. Experimental Section

Chemical Modification: The chemical reaction scheme for modification of starch nanoparticles is presented in Figure 1, and described further below. All reactions were repeated in triplicate to account for batch-to-batch variability.

Chemical Modification—Cationization of Starch Nanoparticles: Starch nanoparticles (StNP-1) were modified to be cationic according to a variation on the procedure shown in Huang et al.[15] Seven grams of starch nanoparticles were dispersed at 0.07 g mL^{-1} into 100 mL of 0.01 g mL^{-1} sodium hydroxide in deionized water. To this dispersion, 3 mL of isopropyl alcohol and 4.3 g (0.5:1 moles based on glycosidic repeat units of starch) of glycidyl trimethyl ammonium chloride were added, and allowed to mix for 1 h. The mixture was then heated to 75 °C and left overnight, before precipitation in anhydrous ethanol and centrifugation, followed by lyophilization, yielding cationic starch nanoparticles (StNP-2).

Chemical Modification—TEMPO Oxidation of Starch Nanoparticles: Starch nanoparticles were oxidized according to a modification of the procedure shown in Kato et al.[16] Briefly, a 100 mL 0.05 g mL^{-1} (5 g or 0.03 mol) dispersion of cationic starch nanoparticles in deionized water was mixed with a 100 mL aqueous solution containing 0.048 g of TEMPO (0.3 mmol) and 0.635 g of sodium bromide (6.2 mmol). The mixture was cooled in an ice bath, and the pH value was adjusted above 10 using a 10% sodium hydroxide solution. Next, 20 g of a 11% sodium hypochlorite solution (1:2 molar ratio to starch nanoparticles) were added slowly to the mixture, while maintaining a pH value above 10. The reaction was continued overnight and the product was precipitated in ethanol and separated by centrifugation, followed by lyophilization to isolate the zwitterionic starch nanoparticles (StNP-3). The same reaction

conditions performed on unmodified starch nanoparticles (StNP-1) yielded anionic particles (StNP-5).

Chemical Modification—EDC/NHS Linkage of FITC-Amine to Carboxylated Starch Nanoparticles: Two grams of zwitterionic starch nanoparticles were dispersed in a 20 mL solution of 0.1 M MES, 0.5 M NaCl buffer. A 10-fold molar excess of EDC was added (0.2 g) over 20 min, followed by the addition of a 1.5-fold mass excess of NHS (0.3 g). A 20 mL solution of 0.1 M PBS, 0.15 M NaCl was added to raise the pH value above 7. Fluoresceinamine was added at a 1:75 molar ratio (0.05 g), and allowed to react for 2 h. The particles were precipitated in ethanol, separated by centrifugation, and lyophilized, yielding fluorescein-labeled cationic starch nanoparticles (StNP-4). The same reaction conditions using the anionic starch nanoparticles (StNP-5) as a starting material yielded fluorescein-labeled anionic particles (StNP-6).

Chemical Analysis: FTIR spectroscopy was performed using a Thermo Scientific Nicolet 6700 instrument. Samples were prepared by spin coating dispersion of modified starch nanoparticles onto a gold-coated silicon wafer, followed by vacuum drying for 24 h. 128 scans were collected for each sample.

^{1}H NMR analysis was performed using a Varian MR400 instrument. Samples were dispersed in D_2O at ≈5% solids and resonance peak positions and integrations were compared to results from the literature.[16]

XPS was run on lyophilized dry powder starch nanoparticle samples using an Axis Ultra X-ray photoelectron spectrometer (Kratos Analyticals, UK) equipped with a monochromatized Al Kα X-ray source at a power of 150 kW.

Particle Characterization: Starch nanoparticle samples StNP-1 – StNP-6 were dispersed in 0.01 M phosphate buffered saline solution at 2.5×10^{-4} g mL^{-1} and analyzed by zeta potential and DLS analysis using a Malvern ZetaSizer, and NTA using a NanoSight NS300. All samples had a pH of 7.4 and were measured at 25 °C. The zeta potential measurements were conducted by inserting 1 mL of the dispersed nanoparticle formulations into a folded capillary cuvette and run using a standard protocol on the Malvern ZetaSizer, involving three repeat measurements to ensure repeatability. DLS measurements were performed by inserting 1 mL of the dispersed nanoparticle formulations into a polystyrene cuvette and running a standard protocol on the ZetaSizer. NTA size measurements were performed by injecting the sample into the flow chamber and completing three 30 s video measurements, leading to a cumulative of thousands of individual particle size measurements for each sample condition.

Particle Degradation Study: Starch particles were dispersed at 0.01 g mL^{-1} in deionized water. Half of the particle dispersions were set aside as an initial dispersion and diluted at a 1:1 ratio with DI-water. The remaining half of the particle dispersions were taken and diluted at a 1:1 ratio with saliva, and placed in an incubator at 37 °C for 30 min. Saliva was collected (donated; human subject exempt) and used immediately to minimize potential denaturation of salivary enzymes. Both the initial and final dispersions were tested with iodine and Benedict's reagent.

Particle Degradation Study—Iodine Test: 20 µL of iodine solution were added to 2 mL of the initial and final dispersions, and examined for color using ImageJ software.[20]

Particle Degradation Study—Benedict's Reagent Test: 20 µL of Benedict's reagent were added to 2 mL of the initial and final dispersions and heated to 80 °C for 30 min, and then evaluated with a UV–vis spectrophotometer to measure absorbance at a wavelength of 735 nm.

TOX8 Cellular Toxicity Assay: Starch nanoparticle samples StNP-1–StNP-6 were evaluated for cellular toxicity with a TOX8 (Resazurin based) assay on HeLa cells. The assay was performed according to manufacturer's instructions with appropriate controls. Cells were seeded in 96 well microtiter plates (1×10^4 cells per 200 µL growth medium per well) followed by overnight incubation. Supernatants from the wells were aspirated out and fresh aliquots of growth medium (containing StNP in desired concentrations in the range of 0.1–10 mg mL^{-1}) were added. After 2 h incubation time, supernatants were aspirated out and the cell monolayers in the wells were washed with 200 µL PBS (0.1 M, pH 7.4). Subsequently, TOX8 reagent (20 µL) was added in each well, incubated for 3 h and fluorescence was recorded at a wavelength of 590 nm using an excitation wavelength of 560 nm using the plate reader, allowing for calculation of cell viability for each well. Each concentration was evaluated in triplicate to assess experimental variability.

Dental Testing—Preparation of Teeth: Extracted teeth were obtained from the School of Dentistry, University of Michigan (human subject exempt) and stored in 0.01 g mL^{-1} sodium azide before use. The teeth were coated with an acid resistant varnish leaving a 1 mm^2 enamel window on the buccal surface of the crowns of the teeth. The teeth were then immersed in a pH 5.0 demineralization gel containing 0.1 M lactic acid, 4.1×10^{-3} M $CaCl_2$-$2H_2O$, 8×10^{-3} M KH_2PO_4, and 1% w/v carboxymethylcellulose sodium at 37 °C for 8 d.[23] At the completion of demineralization, the teeth were rinsed with DI-water before subjection to caries activity testing. Residual varnish was removed by washing in acetone.

Dental Testing—Cavity Diagnosis Testing: For caries testing, 0.01 g mL^{-1} solutions of FITC-dextran, StNP-4, and StNP-6, and a 10^{-5} g mL^{-1} solution of fluorescein sodium salt were prepared. Teeth were exposed to 20 µL of sample for 3 min prior to rinsing in DI water. Rinsing proceeded for 10 s, and the teeth were examined and photographed, while illuminated with a dental curing light. Rinsing was then continued for an additional 10 s, followed by imaging, and this was repeated for up to 5 min to determine residence times for each sample used to optimize the exposure and rinsing procedure.

A 20 s rinse in DI water was sufficient to wash away all but the cationic fluorescent StNPs, which remained even up to 5 min. Fifteen teeth were divided into 3 groups of 5 for testing with each control (fluorescent FITC-Dextran, anionic fluorescent StNP, and fluorescein sodium salt). After a 3 min exposure followed by 30 s of rinsing, imaging was performed under illumination by the dental curing light. The same teeth were then dosed with fluorescein-labeled cationic StNPs and imaged to demonstrate the ability of these particles to illuminate the carious lesions that could not be lit by the various controls.

Dental Testing—Remineralized Lesions Activity Testing: Prior to remineralization, active lesions were illuminated with StNP-4 to obtain a baseline readout. These demineralized teeth were then remineralized by immersion in a remineralization solution containing 0.02 M cacodylic acid sodium salt, trihydrate, 1.5×10^{-3} M $Ca(NO_3)_2$-$4H_2O$, 0.9×10^{-3} M NaH_2PO_4-H_2O, 150×10^{-3} M KCl, and 0.05 ppm NaF, with pH value adjusted to 7.0.[22] Teeth were immersed at 37 °C for 13 d. Images of remineralized teeth were taken for analysis prior to, and after exposure to cationic fluorescent StNPs.

Dental Testing—Image Analysis: Digital images were taken with a Canon DS126061 DSLR camera with a Sigma 105 mm 1:2.8 DG Macro lens and analyzed using ImageJ image analysis software. This provided RGD images and ImageJ image analysis techniques were used to compare the brightness of the carious lesion relative to the background tooth. Green pixel images were then extracted using ImageJ software and analyzed by the same methods. Digital images were also taken with a Fluorchem M Imaging system, with auto-exposure, blue light illumination and a green 542 nm bandpass filter applied to validate the particle fluorescence in the carious lesions, and analyzed using the same methods with ImageJ image analysis software.

Dental Testing—Two-Photon Microscopy: Treated teeth were examined using a Leica TCS SP8 Two-Photon Confocal Microscope equipped with FLIM & FCS capabilities using a 40X oil-immersion objective. Samples were immersed in oil and placed on a glass-bottomed petri dish. The illumination wavelength was set to 810 nm, and z-stack images were collected for a variety of tooth samples.

Supporting Information

Supporting Information is available from the Wiley Online Library or from the author.

Acknowledgements

The authors acknowledge analytical support from K.C. Chang (XPS), M. Bodner (FTIR), B. Plummer (Tox8 assay), and L. Barthel (two-photon microscopy). The authors further acknowledge financial support from Colgate-Palmolive. The authors thank EcoSynthetix Inc. for providing experimental grade starch nanoparticles. The authors thank Dr. Steven Bloembergen (Chairman and CEO of GreenMark Biomedical Inc.) for his valuable comments and advice throughout the study. N.J. acknowledges the National Science and Engineering Research Council of Canada for financial support through a PGS-D fellowship.

Received: August 8, 2016
Revised: October 3, 2016
Published online: November 15, 2016

[1] J. Vasir, V. Labhasetwar, *Technol. Cancer Res. Treat.* **2005**, *4*, 4.
[2] S. Parveen, R. Misra, S. Sahoo, *Nanomed.: Nanotech. Biol.Med.* **2012**, *8*, 2.
[3] A. C. Misra, S. Bhaskar, N. Clay, J. Lahann, *Adv. Mater.* **2012**, *24*, 28.
[4] WHO Media Centre, *Oral Health Fact Sheet*, http://www.who.int/mediacentre/factsheets/fs318/en/ (accessed: October 2015).
[5] NIHNIDCR, *Dental Caries Statistics*, http://www.nidcr.nih.gov/DataStatistics/FindDataByTopic/DentalCaries/ (accessed: October 2015).
[6] B. Clarkson, J. Wefel, L. Silverstone, *Caries Res.* **1981**, *15*, 158.
[7] J. Featherstone, *J Dent. Res.* **2004**, *83*, Spec No C:C39–42.
[8] K. Thoma, in *The American Textbook of Operative Dentistry*, 7th ed. (Ed: M. Ward), Lea & Febiger, Philadelphia, USA **1940**, Ch. 29.
[9] J. B. Summit, J. W. Robbins, R. S. Schwartz, *Fundamentals of Operative Dentistry: A Contemporary Approach*, 2nd ed. Quintessence Publishing Co., Carol Stream, IL, USA **2001**.
[10] A. I. Ismail, ICDAS Coordinating Committee, in *Proceedings of the 7th Indiana Conference*, (Ed: G. Stookey), Indianapolis, USA **2005**, p. 161.
[11] R. I. Ferreira, F. Haiter-Neto, C. P. Tabchoury, G. A. de Paiva, F. N. Bóscolo, *Braz. Oral Res.* **2006**, *20*, 114.
[12] J. D. Bader, D. A. Shugars, G. Rozier, K. N. Lohr, A. J. Bonito, J. P. Nelson, A. M. Jackman, *AHRQ Evidence Report Summaries* **2001**.
[13] M. Zeitouny, M. Feghali, A. Nasr, P. Abou-Samra, N. Saleh, D. Bourgeois, P. Farge, *Sci. World J.* **2014**, *2014*, 924741.
[14] T. Hara, N. Imami, T. Hara, *Am. J. Opthalmol.* **1998**, *126*, 4.
[15] Y. Huang, M. Liu, C. Gao, J. Yang, X. Zhang, X. Zhang, Z. Liu, *Int. J. Biol. Macromol.* **2013**, *58*, 231.
[16] Y. Kato, R. Matsuo, A. Isogai, *Carbohydr. Polym.* **2003**, *51*, 69.
[17] J. Bendoraitiene, R. Kavaliasukaite, R. Klimaviciute, A. Zemaitaitis, *Starch* **2006**, *58*, 12.
[18] W. Pi-Xin, W. Xiu-Li, D. H. Xue, K. Xu, Y. Tan, X. B. Du, W. B. Li, *Carbohydr. Res.* **2009**, *344*, 7.
[19] V. Filipe, A. Hawe, W. Jiskoot, *Pharm. Res.* **2010**, *27*, 5.
[20] K. Mathews, J. Landmark, D. Stickle, *J. Chem. Educ.* **2004**, *81*, 5.
[21] S. K. Fischer, F. Piller, *Staerke* **1978**, *30*, 4.
[22] J. R. S. Maas, I. M. Faraco Junior, C. S. Lodi, A. C. B. Delbem, *Int. J. Paediatr. Dent.* **2013**, *23*, 166.
[23] H. M. Nassar, F. Lippert, G. J. Eckert, A. T. Hara, *Caries Res.* **2014**, *46*, 557.

